THE STEADY THERMODYNAMICS OF A FLASH-BINARY GEOTHERMAL POWER SYSTEM BASED ON CORRECTION MODELS VALIDATED BY STATIC TESTS

Chao LUO[*a,b,c,d], *Hongmei YIN*[a], *Jun ZHAO*[a], *Qingsong AN*[a] *Yulie GONG*[b,c,d]

[*a] Key Laboratory of Efficient Utilization of Low and Medium Grade Energy (Tianjin University), Ministry of Education, Tianjin 300350, China; [b] Guangzhou Institute of Energy Conversion，Chinese Academy of Sciences，Guangzhou 510640，Guangdong, China; [c] Key Laboratory of Renewable Energy，Chinese Academy of Sciences，Guangzhou 510640，Guangdong, China; [d] Guangdong Provincial Key Laboratory of New and Renewable Energy Research and Development, Guangzhou 510640，Guangdong, China;

[*] Corresponding author; E-mail: luochao@ms.giec.ac.cn

The operation parameters and performance of a flash-binary power system are analyzed based on four scenarios of the experiment (Exp), optimum design (OD), error correction model 1 (ECM1) and error correction model 2 (ECM2). The operation parameters of a flash-binary power system are tested to explain steady in the experiment with heat source temperature ranges from 100°C to 150°C. The results show that the simulation data of error correction model 2 have a good agreement with the experiment and most parameter values of relative error δ are less than 5%. The expander with low isotropic efficiency results in the largest exergy losses in the flash-binary power system. The flash-binary power system has better performance to adapt to the mid-high temperature geothermal resource in China. Some valuable data obtained from the research can be applied in the future power plant construction in China's southern Tibet, western Yunnan and Sichuan.

Key words: *mid-high geothermal resource; flash-binary system; steady and thermodynamics; exergy losses*

1. Introduction

With rapid industrialization in China, the fog-haze pollutions are a serious challenge for people, the gas emissions from coal combustion power plants being one of the reasons for fog-haze pollutions [1-3]. Geothermal energy is Environment-friendly compared with fossil fuels. The amount of pollutions from a geothermal power plant is very low, such as CO_2, H_2S and haze emission. There are no pollutions to the atmosphere for a closed cycle of geothermal binary power plant [4-5]. The geothermal resource could be classified into high, medium and low enthalpy resources according hydrothermal systems temperature. When the temperature of the geothermal fluid is above 150^{o}C, it is a high enthalpy resource; when the temperature of the geothermal fluid is between100^{o}C and150^{o}C, it can be defined as a medium enthalpy resource. When the temperature of the geothermal fluid is below100^{o}C, it is a low enthalpy resource [6-7].

Geothermal resources distributed in China have some characteristics, such as large reserves, wide distribution and low temperature. However, the potential of mid-low geothermal resource utilization is large. In 2015, China Geological Survey, affiliated to the Ministry of Land and Resources (MLR),

released the survey results, which evaluated that the reserve of hydro-geothermal resources are equivalent to 1250 billion tons of standard coal, and the available amount of hydro-geothermal resources per year are equivalent to 1.9 billion tons of standard coal [8].The mid-high temperature geothermal resources are mainly distributed in southern Tibet, western of Yunnan and Sichuan in China. However, the installed capacity of geothermal power generation in China is only 27.78MWe. It is the obligation and responsibility for the Chinese government to develop the geothermal resource. By 2020, the installed capacity of geothermal power mainly distributed in Tibet, Sichuan and Yunnan, will be increased to 530MW [9].

The most common geothermal power plants are: (a) Dry steam power generation system; (b) Single and double flash power generation system; (c) Binary power generation system based on Organic Rankine Cycle (ORC) or Kalina cycle [10]. Flash-binary power generation system combines the single flash and binary cycle, and has the benefits of the two power generation types, such as high utilization efficiency of the geothermal resource. It has been a hot topic for researchers to exploit the mid-high geothermal resource. The residual brine from the separator of Dieng single-flash geothermal power plant was designed to utilize for the binary cycle, which can generate electricity up to 20 MW. The limitation factors, such as flashing pressure, evaporating pressure, pinch-point temperature difference, rejection temperature, and heat transfer coefficient in the heat exchanger, were considered in optimization of a flash-binary power system [11]. The average levelized cost per unit of exergy power was proposed to discuss and optimize the flash-binary system. The results showed that the most exergoeconomically effective system couldn't get the optimum thermodynamic parameters of system and vice versa [12]. The multi-objective optimization method based on Pareto optimal solutions was used in Sabalan geothermal power plant in Iran. The results show that exergy efficiency of the flash-binary system is better than the single and double flash system [13]. Single flash/ORC combined systems with different organic fluids are analyzed from energy, exergy, exergoeconomic and thermoeconomic points. The results show that the flash-binary system had a higher first low efficiency, exergy efficiency and unit cost of produced power compared with the double flash system [14]. For water-dominated geothermal resource, when the temperature ranges from 110 to 160^{o}C, an important merit parameter was recommended as an objective function for optimal design, which can be considered, is the mass flow rate to generate a fixed power output, or specific brine consumption [15]. Three compound geothermal power generation systems (double flash, falsh-binary, and double flash-binary) can increase up to 20% power output compared with the single-flash system on the same conditions of geothermal resource [16]. In addition, the choice of working fluids was researched for flash-binary system, mainly focus on thermodynamic and economic performance. Zeyghami [17] pointed out the performance indexes and organic working fluid selection of the flash-binary geothermal system; various working fluids are suitable to the flash-binary system when the geothermal resource temperature between 150 ^{o}C and 250 ^{o}C.

Experimental investigations were conducted to research and verify the performance of small capacity of ORC power system, and the simulation heat source temperature is usually below 100 ^{o}C. The results showed that the first law efficiency of experimental ORC system will increase with higher simulation heat source temperature, when the mass flow rate is constant [18]. However, the cost of small scale expander in the ORC system is too much expensive, which is about more than1500 $/kW. One of the reasons for the high price is that the application of small capacity expander is not commercialized. The cost will decrease with large-scale application of expander. In some experiments,

the expander of the ORC system is replaced by a modified reversed compressor [19, 20]. With the popularity of ORC research, more and more companies in the refrigeration area are starting to conduct ORC research. A modified scroll expander is used in the experiment, the result showed that the shaft and electricity power output were 1.74kW and 1.375 kW respectively when the working fluid is R245fa [21]. Quoilin et al. [22] built a prototype of the ORC system, an open-drive oil-free scroll expander was used in the prototype, and the working fluid is R123. Fortunately, the isentropic efficiency of the expander was up to 68%.

The flash-binary power system is proposed for mid-high temperature geothermal resource distributed in southern Tibet, western Yunnan and Sichuan. The model is corrected by experimental data. The experimental results can provide optimum design opinions of future mid-high geothermal power plant construction in China.

2. Thermodynamic calculations and performance indicators

The flash-binary geothermal power system is composed of a single flash and binary cycle subsystems. The main equipment includes high temperature water boiler, steam separator, flash system expander, evaporator, preheater, binary cycle expander, working fluid pump, condenser and cooling tower. The mid-high temperature simulated water with 100-150 ^{o}C is vaporized partially when the hot saturated water flows through the throttle valve. Steam/water two-phase mixture enters the separator, and the separated saturated steam flows into the shut-off valve in the flash power subsystem, the separated saturated water flows into the evaporator in the binary power subsystem. The separated saturated steam is condensed by cooling water and drained to the water tank. The separated saturated water flows into the evaporator, the preheater and finally into the boiler. The flow process of working fluid R245fa is a closed cycle. The liquid R245fa in the fluid tank is pumped to preheater, and then flows into the evaporator. The superheated vapor of R245fa heated by the separated water in evaporator enters into the binary cycle expander, and pushes the turbine to rotate, which drives the generator to generate electricity. The R245fa vapor is finally condensed by cooling water.

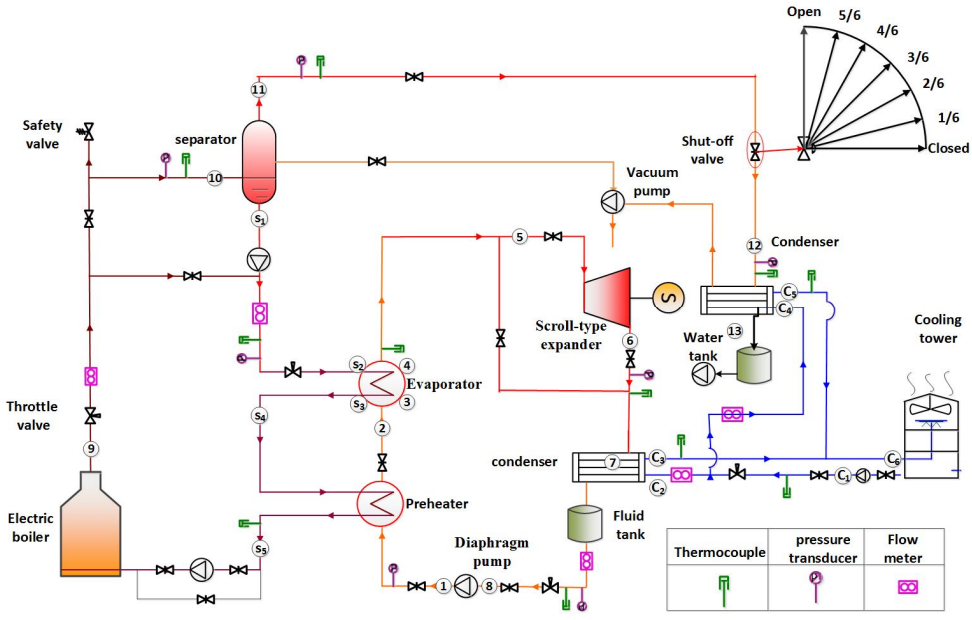

Figure. 1 Schematic diagram of flash-binary system

The temperature-entropy (*T*-*s*) diagram of the flash-binary power system is shown in figure 2. The *T* represents Celsius temperature of different states and the *s* represents entropy of different states. The numbers showing the thermodynamic states in Fig. 2 are consistent with those in Fig. 1. Path 11–12 and 5-6 show the real process of the steam in the turbine, and path 11-12s and 5–6s denote the isentropic process of the steam.

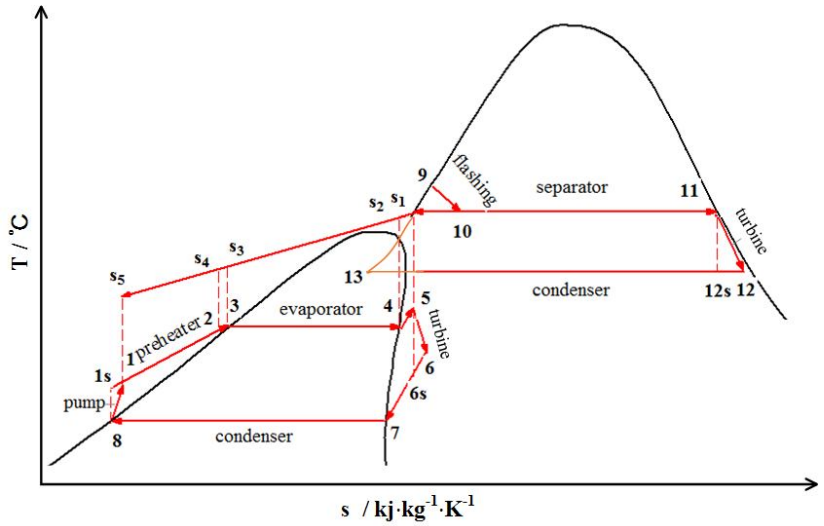

Figure. 2 Temperature-entropy diagrams of the flash-binary power system

The available thermodynamic cycles of the flash-binary power system can be divided into nine main groups:

Heat source boiler:

$T_9 = T_{\text{source}}$ (1)

$m_9 = m_{\text{source}}$ (2)

$m_9 h_9 = m_{s5} h_{s5} + W_{boiler}$ (3)

Condenser for single flash subsystem:

$p_{13} = p_{Con}$ (4)

$T_{C4} = T_{C1}$ (5)

$T_{C5} = T_{C4} + \Delta T_C$ (6)

$m_{12}(h_{12} - h_{13}) = m_{C4}(h_{C5} - h_{C4})$ (7)

Separator for single flash subsystem:

$p_{sep} = p_{10} = p_{11} = p_{s1}$ (8)

$h_9 = h_{10}$ (9)

$m_9 = m_{10}$ (10)

$m_{10} = m_{11} + m_{s1}$ (11)

$m_{10} h_{10} = m_{11} h_{11} + m_{s1} h_{s1}$ (12)

Expander for single flash subsystem:

$p_{Con} = p_{12}$ (13)

$m_{11} h_{11} = m_{12} h_{12} + W_{flash}$ (14)

$$\eta_{F,turbine} = \frac{h_{11} - h_{12}}{h_{11} - h_{12,s}} \quad (15)$$

$h_{12,s}$ is the isentropic enthalpy of the water steam for the process 11-12s.

Condenser for binary cycle subsystem:

$$p_{Con} = p_7 = p_8 \quad (16)$$

$$T_{C2} = T_{C1} \quad (17)$$

$$T_{C3} = T_{C2} + \Delta T_C \quad (18)$$

$$m_8(h_7 - h_8) = m_{C2}(h_{C3} - h_{C2}) \quad (19)$$

Working pump for binary cycle subsystem:

$$\eta_{pump} = \frac{100(P_1 - P_8)}{\rho_8(h_1 - h_8)} \quad (20)$$

$$W_{pump} = m_8(h_1 - h_8) \quad (21)$$

Evaporator for binary cycle subsystem:

$$p_{vap} = p_1 = p_2 = p_3 = p_4 = p_5 \quad (22)$$

$$p_{s1} = p_{s2} = p_{s3} = p_{s4} = p_{s5} \quad (23)$$

$$m_{s1} = m_{s2} = m_{s3} = m_{s4} = m_{s5} \quad (24)$$

$$m_3(h_4 - h_3) = m_{s2}(h_{s2} - h_{s3}) \quad (25)$$

Preheater for binary cycle subsystem:

$$T_2 = T_3 - \Delta T_{sub,vap} \quad (26)$$

$$m_1(h_2 - h_1) = m_{s4}(h_{s4} - h_{s5}) \quad (27)$$

Expander for binary cycle subsystem:

$$p_{Con} = p_6 \quad (28)$$

$$T_5 = T_4 + \Delta T_{super,vap} \quad (29)$$

$$m_5 h_5 = m_6 h_6 + W_{binary} \quad (30)$$

$$\eta_{B,turbine} = \frac{h_5 - h_6}{h_6 - h_{6,s}} \quad (31)$$

$h_{6,s}$ is the isentropic enthalpy of the R245fa vapor for the process 5-6s.

The first and second law efficiencies are usually used to evaluate the performance of geothermal power system, they can be given by:

$$\eta_1 = \frac{W_{net}}{m_9(h_9 - h_{s5})} = \frac{W_{binary} + W_{flash} - W_{pump}}{m_9(h_9 - h_{s5})} \quad (32)$$

$$\eta_2 = \frac{W_{net}}{m_9 e_9} = \frac{W_{binary} + W_{flash} - W_{pump}}{m_9[(h_9 - h_0) - T_0(s_9 - s_0)]} \quad (33)$$

h_0 and s_0 are reference enthalpy and entropy respectively.

The geothermal temperature is one of the factors to affect the first and second low efficiency. However, some other indications could be obtained for geothermal power plant by recombining related parameters, such as heat source, rejection geothermal water temperatures and cooling water temperature. Therefore, another significant indication is proposed in this paper. That is the ratio between a fixed power output and the mass flow rate, or specific net power output, which is given by:

$$Ne = \frac{W_{net}}{3.6 m_9} \quad (34)$$

The parameter Ne is often considered when the maximization of net power output for a given mass flow rate is suggested as an objective function for the optimal design.

3. Optimal methodology and experimental test

3.1. Optimal methodology

The optimal design of a flash-binary geothermal power plant is a multi-objective, multi-variable constrained optimization problem. The initial parameters related to the system performance had to be defined, i.e. the heat source and ambient temperature, the mass flow rate, and the cooling water temperature. An assumed value is given to the initial condenser pressure for iteration calculation and the final condenser pressure will be constrained by pinch-point temperature difference. The optimum flash and evaporator pressure will be defined by maximizing the specific net power output (Ne). The performance and operation parameters will be analyzed on the condition of optimum flash and evaporator pressure. The schematic diagram of the optimum design procedure is given in figure 3.

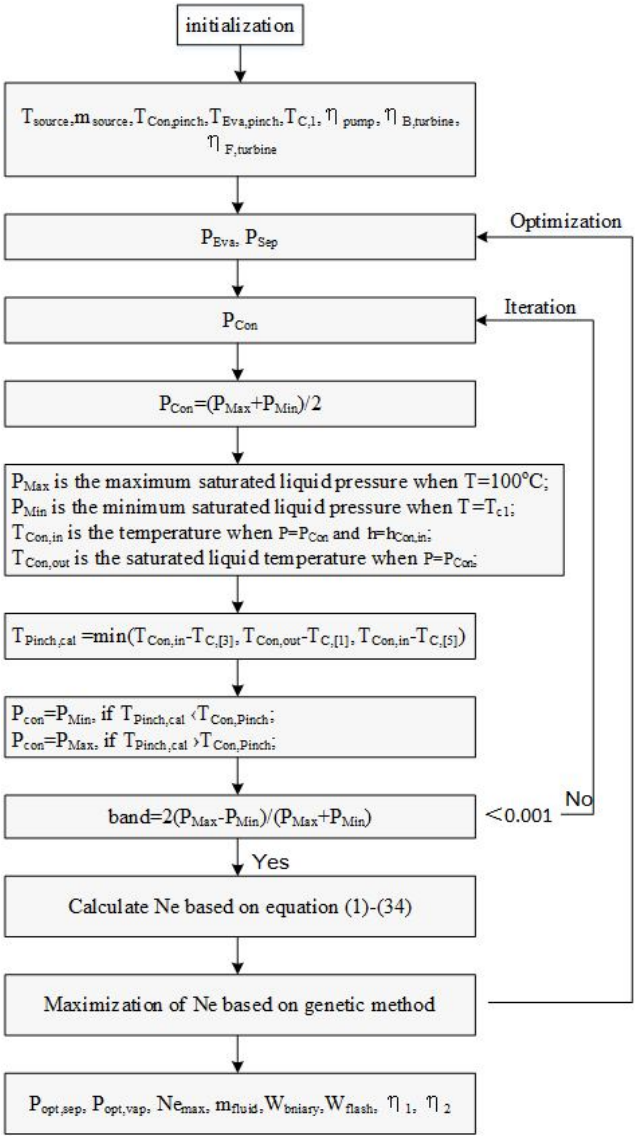

Figure. 3 Schematic diagram of the optimum design procedure

3.2. Experiment test

The research of the flash-binary power system will provide proposals in China for the mid-high temperature geothermal resource, such as Tibet, Sichuan and Yunnan province. The test bench data will be verified the reliability and steady of the flash-binary power system model. Figure 4 gives the

main subsystem and equipment's photographs of flash-binary system. The main subsystem includes single flash and binary cycle system. The high temperature and pressure water heated by electricity can be produced by the boiler (AEWT/H-30-80), and 100-150^{o}C high temperature water will be produced continuously; the water and gas will be fed by the soft water and compressor for the heating system. Small scale capacity expanders with a lower cost are not found in the market in China. Therefore, a modified compressor is used as an expander in the binary subsystem, and the compressor has to install with opposite direction. The expansion process of the flash power subsystem is replaced by throttling process.

The major components in the single flash subsystem are throttled valve, vacuum pump, separator and condenser. The working fluid pump is a diaphragm pump (SJ3-M-630/1.5) which could control the mass fluid of R245fa. A scroll-type compressor is modified to the expander. The LED bulbs are used as output power consumed loads.

Figure. 4 Photographs of flash-binary system test

4. Experimental procedure and error correction model

4.1. Experimental procedure

The experiment process must be operated carefully because the parameters are sensitive by adjusting the valve. The experimental procedures are as follows：

(1) Turn on the power switch of cooling pump. The cooling loop of the flash and binary subsystem will operate first;

(2) Turn on the electric heating copper switch on the boiler. The high temperature and pressure water will be produced;

(3) Turn on the power switch of the hot water pump and vacuum pump. The hot water flows into the flasher and is separated into steam and water. The flash power system will operate stably with 10 mins;

(4) Turn on the power switch of working fluid pump. The evaporate pressure will increase with heated R245fa. Open the valve in front of the expander when the R245fa vapor at a super heat state;

(5) Adjust the mass flow rate of R245fa and observe the operation parameters. The data will be recorded when the power output is stable. The opening fraction of the shut-off valve in the flash subsystem has to adjust when the hot water temperature higher than 120 ^{o}C because of the vibration of the boiler, which is due to the feeding process of water and gas by the soft water and the compressor in the boiler. Therefore, the opening fraction is adjusted manually larger than 1/6 to prevent boiler vibration when the heat source water temperature is higher than 120^{o}C;

(6) Reset the heat source temperature from 100 °C to 150 °C, and repeat the steps from (1) to (5).

Some measuring instruments are used in the experiment. PT100 and pressure transducers are used to measure the temperature and pressure respectively. Coriolis flowmeter and electromagnetic flowmeter are used to measure R245fa and water mass flow rate. The test data are transported to the paperless recorder by the data line and saved in the computer finally.

4.2. Error correction model

The experiment (Exp) and optimum design (OD) initial conditions are different because of experimental equipment limitations (i.e. turbo compressors) and cold sources temperature difficult to control. Therefore, error correction models are proposed based on experimental conditions. The error correction model 1 (ECM1) corrected the pinch point difference to 4°C. The error correction model 2 (ECM2) corrected the isotropic efficiency of binary and flash expender to 0.25 and 0.11 respectively based on ECM1. The relative error is given by formula (35).

$$\delta = \frac{V_{Exp} - V_{ECM2}}{V_{Exp}} \times 100\% \quad (35)$$

The initial and optimum parameters of four scenarios are given in table 1.

Table. 1 The initial and optimum parameters of four scenarios

scenarios	T_9 °C	P_{11} bar	P_5 bar	m_{10} kg/s	T_{c1} °C	Pinch point °C	$\eta_{B,turbine}$ -	$\eta_{F,turbine}$ -
Exp	100~150	test	test	test	test	-	-	-
OD	100-150	optimum	optimum	test	25	8	0.8	0.8
ECM1	100~150	test	test	test	test	4	0.8	0.8
ECM2	100~150	test	test	test	test	4	0.25	0.11

4.3. Initialization parameters

The temperature of cooling water is determined by the factors of the environment. Figure 5 shows the inlet cooling temperature under Exp and OD scenarios. When the heat source temperature ranges from 100 to 150°C, the optimal design cooling water temperature is 25°C, and the actual cooling temperature is 20°C, 22°C, 25°C, 20°C, 20°C and 25 °C on experimental dates.

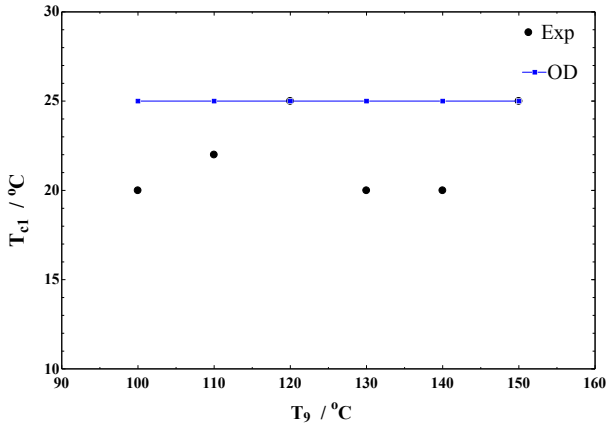

Figure. 5 T_{c1} on the scenarios of Exp and OD

Flash pressure is one of the optimization parameters to maximize specific net power output (Ne). The flash pressure is increasing with higher heat source temperature. Figure 6 gives P_{10} value on the

conditions of OD and Exp scenarios when the heat source water temperature ranges from 100°C to 150°C. The flash pressures are 0.46bar and 0.51bar, 0.605bar and 0.73bar, 0.79bar and 0.81bar, 1.025bar and 0.79bar, 1.139bar and 0.62bar, 1.701bar and 0.73bar respectively on the conditions of OD and Exp scenarios.

The flash separator was customized and the volume of the flash separator has been shaped in the experimental process. The flash pressure P_{10} is adjusted by the opening fraction of the valve which is instead of the expander in the experimental process. When the heat source water temperature ranges from 100°C to 120°C and the valve keeps 1/6 opening fraction, the P_{10} values are close on OD and Exp scenarios. However, when the heat source water temperature ranges from 120°C to 150°C, the P_{10} values are not close on OD and Exp scenarios because the open fraction is adjusted larger than 1/6 in the experimental process. When the heat source water temperature is higher than 120°C, the boiler will appear strong vibration because of the feeding process of water and gas by the soft water and the compressor. Therefore, the opening fraction is adjusted manually larger than 1/6 to prevent boiler vibration when the heat source water temperature is higher than 120°C. The flash pressure on Exp is lower than the OD scenario when the T_9 is higher than 120°C. The trend of P_{10} is associated and similar to T_{c1}.

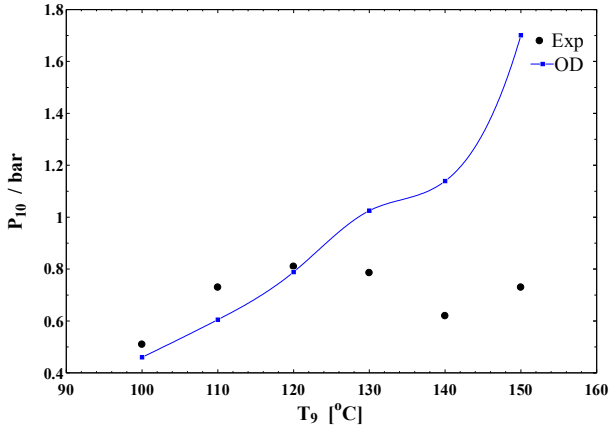

Figure. 6 P_{10} on the scenarios of Exp and OD

The separated saturated water is the heat source of binary power cycle subsystem and the evaporator pressure P_5 is associated with the flash pressure P_{10}. Figure 8 gives the relationship between P_5 and T_9 on the conditions of OD and Exp scenarios. The evaporator pressures are 4.46bar and 6.2bar, 4.93bar and 7.96bar, 5.46bar and 8.46bar, 6.05bar and 7.5bar, 6.71bar and 5.8bar, 7.47bar and 6.7bar respectively on the conditions of OD and Exp scenarios. P_5 increases with higher T_9 on the condition of the OD scenario. The trend of P_5 is similar to P_{10} on the condition of Exp scenario because P_5 is affected by the flash pressure and uncontrolled cooling water temperature in the experimental process.

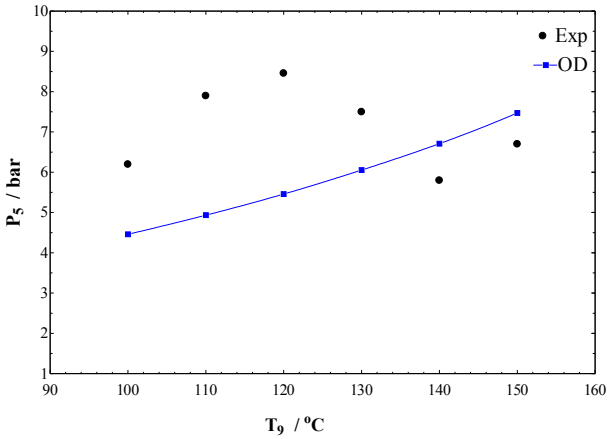

Figure. 7 P_5 on the scenarios of Exp and OD

4.4. Exergy losses

The second low efficiency related to the exergy losses of system. The exergy losses of the power system are:

$$I = I_{sep} + I_{vap} + I_{pre} + I_{Con} + I_{pump} + I_{turbine} + I_{rej} = m_9 e_9 - W_{net} \quad (36)$$

$$I_{sep} = m_9 e_9 - m_{s1} e_{s1} - m_{11} e_{11} \quad (37)$$

$$I_{vap} = (m_{s1} e_{s1} + m_3 e_3) - (m_{s3} e_{s3} + m_5 e_5) \quad (38)$$

$$I_{pre} = (m_{s3} e_{s3} + m_1 e_1) - (m_{s5} e_{s5} + m_3 e_3) \quad (39)$$

$$I_{Con} = [(m_{C4} e_{C4} + m_{12} e_{12}) - (m_{C5} e_{C5} + m_{13} e_{13})] + [(m_{C2} e_{C2} + m_7 e_7) - (m_{C3} e_{C3} + m_8 e_8)] \quad (40)$$

$$I_{pump} = m_1 e_1 - (W_{pump} + m_8 e_8) \quad (41)$$

$$I_{rej} = m_{s5} e_{s5} \quad (42)$$

$$I_{turbine} = [m_{11} e_{11} - (W_{flash} + m_{12} e_{12})] + [m_5 e_5 - (W_{binary} + m_7 e_7)] \quad (43)$$

5. Results and discussion

The operation parameters, performance index and stability of flash-binary power system are analyzed on the Exp, OD, ECM1 and ECM2 scenarios.

5.1. Operation parameters analysis

Figure 8 gives the rejection temperature T_{s5} of the flash-binary power system with heat source water temperature ranges from 100°C to 150°C in four scenarios. In the OD scenario, the T_{s5} increases with increasing T_9 because the flash and the evaporator temperature also increase with higher T_9. The values of T_{s5} have similar trend with P_5 and P_{10} on the Exp scenario, and are 74.3°C, 84°C, 85°C, 80.5°C, 74.5°C and 76.5°C respectively when heat source water temperature ranges from 100°C to 150°C. The values of T_{s5} in the ECM1 scenario are the same with the ECM2, which are 73.67°C, 82.54°C, 85.35°C, 79.45°C, 70.57°C, and 76.02°C respectively. This is mainly due to the fact that the correction values of pinch point temperature difference are the same with ECM2. The data of the experiment and the error correction model are in good agreement in figure 8. The maximum and minimum relative error δ of T_{s5} between Exp and ECM2 are 5.0% and 0.24% respectively.

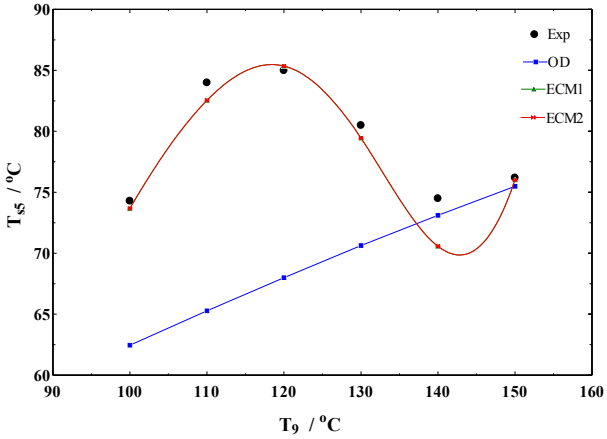

Figure 8 the relationship between P_{s5} and T_9 on four scenarios

The expanders exhaust gas temperature of binary cycle T_6 and flash power system T_{12} in four scenarios are given in figure 9(a) and 9(b). T_6 and T_{12} are determined by the condenser temperature and isotropic efficiency of the expander. T_6 and T_{12} are 51.35°C and 43°C respectively with increasing T_9 in the OD scenario, however, T_6 and T_{12} have a large gap between the experimental and the design data because of the different condenser temperature and isotropic efficiency. The curves of T6 and T12 have the same trend in the Exp, ECM1 and ECM2 scenarios. When the hot source water temperature ranges from 100°C to 150°C, the T_6 and T_{12} are 54°C and 60°C, 63°C and 67.5°C, 66°C and 67.5°C , 62°C and 68.5°C, 57.5°C and 64°C, 58 °C and 67°C respectively in the Exp scenario. The data of T_6 and T_{12} have deviation between Exp and ECM1 scenarios because the condenser pinch point difference is only corrected in the ECM1. However, the data of T_6 and T_{12} on ECM2 scenario are close to Exp because the condenser pinch point difference and isotropic efficiency are both corrected in the ECM2. The data of T_6 and T_{12} are 55.7°C and 56.3°C, 61.7°C and 62.2°C, 64.2°C and 65°C, 59.9°C and 62.4°C, 54.9°C and 59.9°C, 59 °C and 63.6°C respectively in ECM2 scenario when heat source temperature ranges from 100°C to 150°C. The maximum and minimum relative error δ of T_6 and T_{12} between Exp and ECM2 are 4.5% and -1.7%, 8.9% and 3.7% respectively.

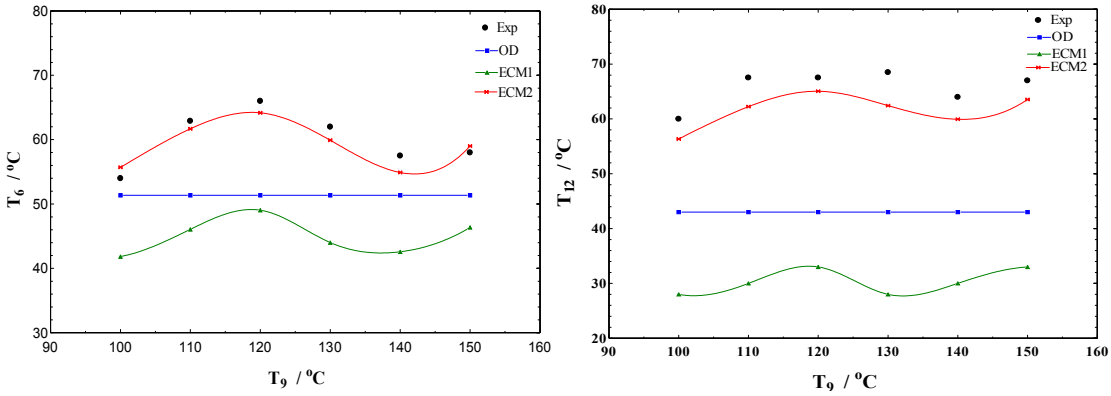

(a) Relationship between T_6 and T_9 (b) Relationship between T_{12} and T_9

Figure 9 the relationship between the expanders exhaust gas temperature and T_9 in four scenarios

5.2. Performance analysis

The specific net power output (Ne) is an important performance parameter of the power system. Figure 10 gives the relationship between Ne and T_9 in four scenarios. The Ne increases with increasing T_9, and the higher T_9 is, the larger increment of Ne, that is the curve slope of Ne becomes larger with

higher T_9 in the OD scenario, which shows that it has better performance for the flash-binary power system to adapt the high-temperature geothermal resource. The values of Ne are 2.759kWh/t, 3.83kWh/t, 5.07kWh/t, 6.481kWh/t, 8.064kWh/t and 9.82kWh/t respectively when T_9 ranges from 100°C to 150°C in OD scenario.

The Ne curve of ECM2 agrees well with the experimental data. The values of Ne are 0.62kWh/t and 0.66kWh/t, 0.7119kWh/t and 0.7262kWh/t, 0.8649kWh/t and 0.908 kWh/t, 1.352kWh/t and 1.374kWh/t, 1.586kWh/t and 1.572kWh/t respectively in ECM2 and Exp scenarios, When T_9 ranges from 100°C to 150°C. The maximum and minimum relative error δ of Ne between Exp and ECM2 are 4.8% and -0.9% respectively. The absolute value of the relative error δ is less than 5%.

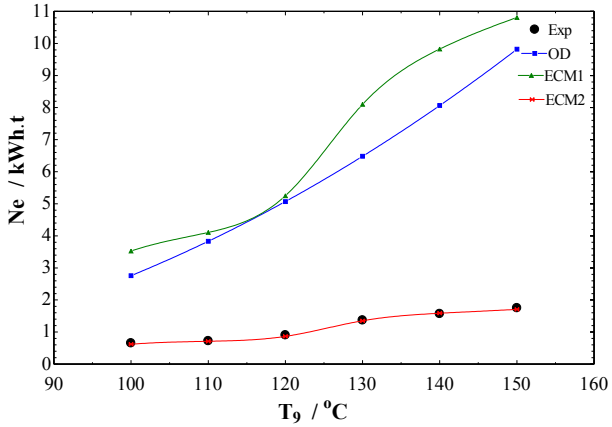

Figure 10 the relationship between Ne and T_9 in four scenarios

5.3. Stability analysis

The stability of the experimental power system is mainly to analyze the fluctuation of the operation parameters. The experimental data is analyzed under the condition of T_9=120°C because the flash pressure and the cooling water temperature agree well between Exp and OD scenarios.

The experimental test parameters of m_8, T_{s2}, T_{s5}, P_5 and P_6 with time at T_9=120°C are given in figure 11. In the experiment operation process, the test values of m_8, T_{s2}, T_{s5}, P_5 and P_6 are constant at 0.079kg/s, 96°C, 85°C, 8.5bar and 1.9bar respectively and have good stability.

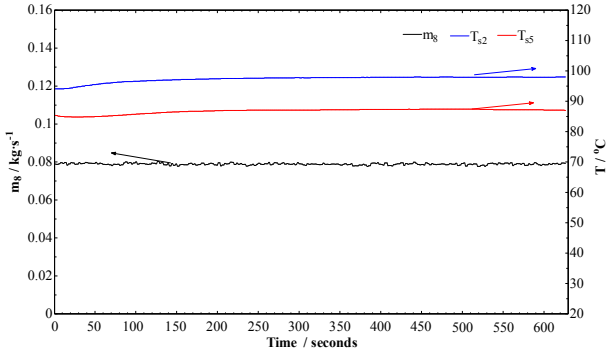

(a) m_8, T_{s2} and T_{s5} with time at T_9=120°C

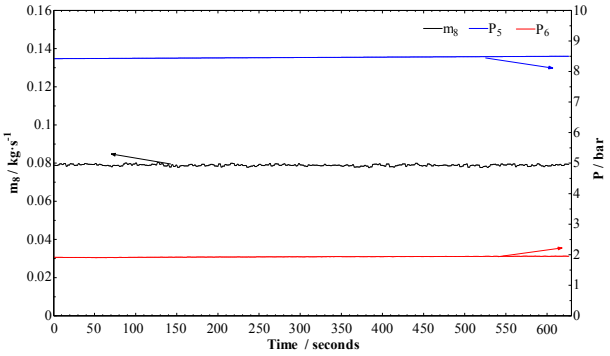

(b) m_8, P_5 and P_6 with time at T_9=120°C

Figure 11 Experimental test data with time at T_9=120°C

The power output of the binary cycle subsystem is tested by the power meter in the experiment. LED light bulbs are used as a load to consume the generated electricity. There are three groups of LED light bulbs with 240W and controlled by an air switch individually. Figure 12 gives the relationship between the output and load power with time at T_9=120°C when load power capacity adjusted. When the capacity of the load power is 240W, the output power capacity of the binary cycle subsystem ranges from 430W to 470W, which is not steady for the binary power subsystem; when the capacity of load power is 480W, the output power capacity of the binary cycle subsystem is constant at 500W, and the brightness of the LED bulbs is suitable; when the capacity of load power is 720W, the output power capacity of the binary cycle subsystem is constant at 640W, and the LED bulbs becomes dim.

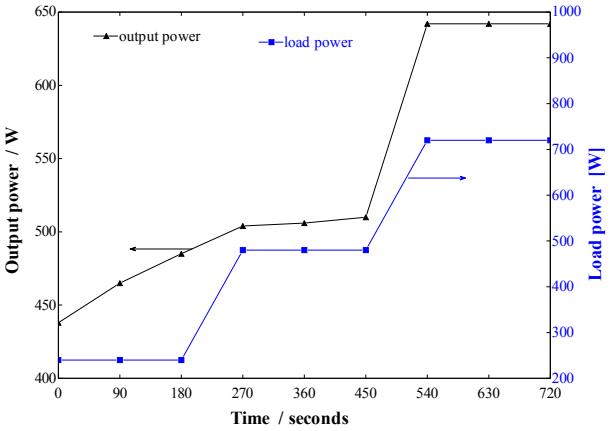

Figure 12 The relationship between output and load power with time at T_9=120°C

6. Exergy analysis

The exergy analysis of the flash-binary power system is analyzed based on ECM2 because the operation parameters and performance of ECM2 have a good agreement with Exp. Figure 13 shows the proportions of the exergy losses in the various components when heat source temperature ranges from 100°C to 150°C. It appears that the turbine with low efficiency, rejection geothermal water at a high temperature, and the condenser are all causes of relatively high exergy losses (41–47%, 33–22% and 16–20%, respectively). Therefore, it is possible to reduce losses in the condenser by changing the pinch point temperature.

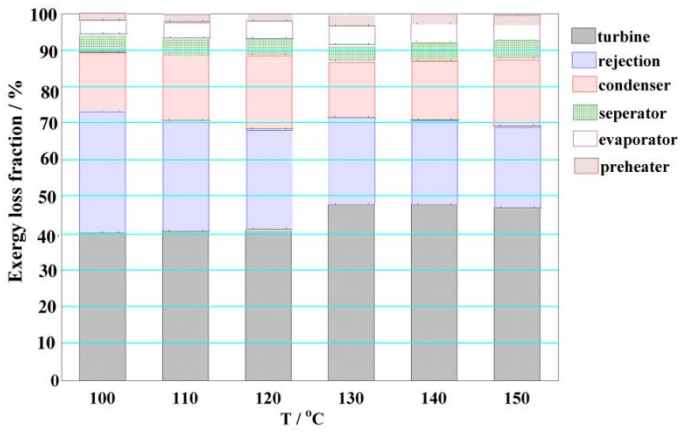

Figure 13 The proportions of the exergy losses in the various components

7. Conclusions

A combined flash-binary experimental prototype of a geothermal power generation system is newly established based on a mid-high geothermal resource in China's southern Tibet, western Yunnan and Sichuan. Some valuable data obtained and can be applied in the future power plant construction from this research, such as:

(1) The operation parameters and performance of ECM2 have a good agreement with Exp. The maximum and minimum relative error δ of T_{s5}, T_6, T_{12} and Ne between Exp and ECM2 are 5.0% and 0.24%, 4.5% and -1.7%, 8.9% and 3.7%, 4.8% and -0.9% respectively;

(2) The flash-binary power system has better performance to adapt to the mid-high temperature geothermal resource in China. The higher heat source temperature is the larger increment of Ne. The increments of Ne are 1.071kWh/t, 1.24kWh/t, 1.411kWh/t, 1.584kWh/t and 1.756kWh/t respectively, for every 10°C increasing of heat source temperature when geothermal temperature ranges from 100°C to 150°C;

(3) The flash and rejection temperature, expander inlet and outlet pressure of the binary cycle subsystem maintain stable values respectively in the process of experiment. When the capacity of load power is smaller than 55% of output power, the output power is not steady for the binary cycle subsystem;

(4) The exergy losses mainly focus on the turbine, the rejection geothermal water and the condenser (41–47%, 33–22% and 16–20%, respectively). The condenser pressure can be optimized in the next step by changing the pinch point temperature.

Acknowledgment

This work is sponsored by National Natural Science Funds (Grant No. 51406212).

Nomenclature

E—exergy, kW;
e —specific exergy, kJ/kg;
h—enthalpy, kJ/kg;
s—entropy, kJ/kg·K;
m—mass flow rate, kg/s;

W_{binary} — power output of binary power subsystem, kW;
W_{flash} —power output of flash power subsystem, kW;
W_{pump} —power consumption of binary power subsystem, kW;
W_{net} — net power output of flash-binary power system, kW;
Ne —specific net power output, kWh/t
P —pressure, bar;
T — temperature, ^{o}C;
V— Values of simulation and test, -;
Greek symbols
η_1 — first law efficiency of flash-binary system, %;
η_2 —exergy efficiency , %;
$\eta_{turbine}$ —isentropic efficiency of expender, %;
Subscripts
1-8 — working fluid state;
9-13 —hot water state;
s1-s5 — separator water state;
c1-c5 — cooling water state;

References

[1] F. Yang, J. Tan, Q. Zhao, Z. Du, et al., Characteristics of PM2.5 speciation in representative megacities and across China, Atmos. Chem. Phys 11 (2011) 5207–5219

[2] Q. Zhang, R. Yan, J. Fan, S. Yu, et al., A heavy haze episode in shanghai in December of 2013: characteristics, origins and implications, Aerosol Air Qual. Res 15 (2015) 1881–1893.

[3] Q. Liu, J. Baumgartner, Y. Zhang, J.J. Schauer, et al., Source apportionment of Beijing air pollution during a severe winter haze event and associated pro-inflammatory responses in lung epithelial cells, Atmos. Environ. 126 (2016) 28–35.

[4] R. DiPippo, Geothermal power plants: principles, applications, case studies and environmental impact. 2nd ed. UK: Butterworth-Heinemann, Elsevier; 2008.

[5] E. E. Michaelides, Alternative energy sources. Berlin: Springer; 2012.

[6] I. Stober, K. Bucher, Geotherma lenergy: from theoretical models to exploration and development. Springer–Verlag 2013.

[7] D. Chandrasekharam, J. Bundschuh, Low-enthalpy geothermal resources for power generation. Taylor&Francis 2008.

[8] [8] J. Hou, M. Cao, P. Liu, Development and utilization of geothermal energy in China: Current practices and future strategies, Renewable Energy 125 (2018) 401-412.

[9] J. Zhu, K. Hu, X. Lu. A review of geothermal energy resources, development, and applications in China: current status and prospects, Energy 93 (2015) 466-483.

[10] E. Efstathios, S. Michaelides, Future directions and cycles for electricity production from geothermal resources, Energy Conversion and Management 107 (2016) 3–9.

[11] A. D. Pasek, T. A. Fauzi Soelaiman, C. Gunawan，Thermodynamics study of flash–binary cycle in geothermal power plant, Renewable and Sustainable Energy Reviews 15 (2011) 5218–5223.

[12] Y. Zhao, J. Wang. Exergoeconomic analysis and optimization of a flash-binary geothermal power system, Applied Energy 179 (2016) 159–170.

[13] A. Aali, N. Pourmahmoud, V. Zare, Exergoeconomic analysis and multi-objective optimization of a novel combined flash-binary cycle for Sabalan geothermal power plant in Iran, Energy Conversion and Management, 143 (2017) 377-390.

[14] N. Shokati, F. Ranjbar, M. Yari. Comparative and parametric study of double flash and single flash/ORC combined cycles based on exergoeconomic criteria, Applied Thermal Engineering 91 (2015) 479-495.

[15] A. Franco, M. Villani, Optimal design of binary cycle power plants for water-dominated, medium-temperature geothermal fields, Geothermics 38 (2009) 379–391.

[16] X. Lu, Y. Zhao, J. Zhu, W. Zhang. Optimization and applicability of compound power cycles for enhanced geothermal systems, Applied Energy 229 (2018) 128–141.

[17] M. Zeyghami, Performance analysis and binary working fluid selection of combined flash-binary geothermal cycle, Energy 88 (2015) 765-774.

[18] L. Li, Y.T. Ge, X. Luo, Experimental investigations into power generation with low grade waste heat and R245fa Organic Rankine Cycles (ORCs), Applied Thermal Engineering 115 (2017) 815-824.

[19] P. Song, M. Wei, L. Shi, A review of scroll expanders for organic Rankine cycle systems, Applied Thermal Engineering 75 (2015) 54-64.

[20] Z. Wu, D. Pan, N. Gao, Experimental testing and numerical simulation of scroll expander in a small scale organic Rankine cycle system, Applied Thermal Engineering 87 (2015) 529–537.

[21] J.C. Chang, C.W. Chang, T.C, Hung, Experimental study and CFD approach for scroll type expander used in low-temperature organic Rankine cycle, Applied Thermal Engineering 73 (2014) 1444–1452.

[22] S. Quoilin, V. Lemort, J. Lebrun, Experimental study and modeling of an organic Rankine cycle using scroll expander, Applied Energy 87 (2010) 1260–1268.